COMMUNICATION

Nitroxyl Radical–Containing Flexible Porous Coordination Polymer for Controllable Size-Selective Aerobic Oxidation of Alcohols

Ping Wang,[a] Ziqian Xue, [a] Ken-ichi Otake[a,*] and Susumu Kitagawa[a,*]

Received 00th January 20xx,
Accepted 00th January 20xx

DOI: 10.1039/x0xx00000x

The ability of flexible porous coordination polymers (PCPs) to change their structure in response to various stimuli has not been exploited in the design of tunable-selectivity catalysts. Herein, we make use of this ability and prepare nitroxyl radical–containing flexible PCP that can reversibly switch between large- and contracted -pore configurations in response to solvent change and thus promote the controllable size-selective aerobic oxidation of alcohols.

Unlike their rigid counterparts, flexible porous coordination polymers (PCPs) exhibit tunable conformations and structural softness due to the reversible nature of coordination bonds and the multitude of possible metal coordination geometries.[1,2] Depending on the guest molecule, pressure, and temperature, flexible PCPs can switch between configurations with different pore sizes and shapes,[3–13] which makes them attractive for applications such as gas separation, storage, and sensing; however, the corresponding catalytic applications remain underexplored.[14–19]

The intriguing catalytic activity of PCPs makes them promising heterogeneous catalysts.[20] In particular, the crystalline porous nature of PCPs allows for size-selective catalysis and catalytic process characterization by crystallographic techniques.[21] Catalytic PCPs exhibit uniform pore structures and are therefore typically more selective than other heterogeneous catalysts. Specifically, catalytic rigid PCPs with a predetermined pore size and shape have been used to achieve substrate selection through strict size sieving and thus realize selective catalytic reactions.[22]

Controllable size-selective catalysis can possibly be realized using flexible PCPs with stimuli-responsive (e.g., solvent-sensitive) pore structures. For example, contracted-pore PCPs can exert a size-sieving effect in catalytic reactions, selectively hosting only small substrates, while expanded-pore PCPs can accommodate both small and large substrates. Thus, flexible PCPs with solvent-sensitive porosity can be used for switchable catalysis (Scheme 1). However, this strategy has not been well explored because of the limited number of stable and flexible PCP catalysts.[23]

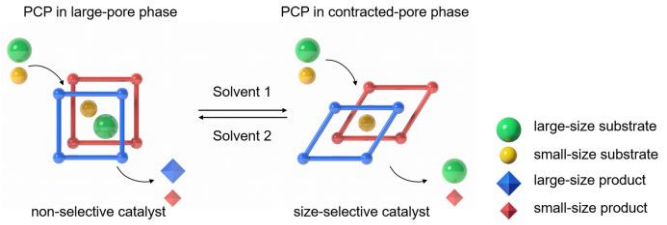

Scheme 1. Flexible catalytic porous coordination polymers with controllable size selectivity. The PCP in the large-pore phase can adsorb various substrates and work as a non-selective catalyst. When PCP changes to the contracted-pore phase, it adsorbs only small-size substrates and becomes a size-selective catalyst.

Herein, we designed and synthesized a radical-containing flexible PCP with size-selective catalytic activity. Organic radicals are efficient catalytic sites but are typically unstable, which complicates their incorporation into PCPs. As typical stable organic radicals, nitroxyl radicals are well-known homogeneous catalysts for the oxidation of alcohols into the corresponding carbonyl compounds.[24] Among the six nitroxyl radical–bearing PCPs reported to date, none combine stability under catalytic conditions with structural flexibility. [25–29] For instance, the UCLA-NO PCP constructed from nitroxyl radical–containing 1,4-bis(4-pyridylethynyl)benzene and a Zn_2 paddlewheel cluster exhibits structural flexibility but decomposes after thermal activation.[29]

Our flexible catalytic PCP was built from two 2,2,6,6-tetramethylpiperidine-1-oxyl (TEMPO)–bearing ligands (Figure 1a), which featured TEMPO moieties linked to [1,1':4',1''-terphenyl]-4,4''-dicarboxylic acid (TPDC) and 1,4-bis(4-pyridinyl)benzene (BPyB) as mobile substituents and were

[a] *Institute for Integrated Cell-Material Sciences (WPI-iCeMS), Kyoto University Institute for Advanced Study (KUIAS), Kyoto University, Yoshida Ushinomiya-cho, Sakyo-ku, Kyoto 606-8501, Japan.*

Electronic Supplementary Information (ESI) available: Experimental procedures, NMR spectra, PXRD, TGA, ESR, crystallographic data, and catalytic characterization. See DOI: 10.1039/x0xx00000x

denoted as TPDC-TEMPO (L1) and BPyB-TEMPO (L2), respectively (Figures S1 and S2). The radical nature of these ligands was confirmed by the presence of a typical three-line signal centered at g = 2.004 in the electron paramagnetic resonance (EPR) spectra of the corresponding methanolic solutions (Figures S3 and S4).

L1 and L2 were treated with a solution of $Zn(NO_3)_2{\cdot}6H_2O$ in a mixture of dimethylformamide (DMF) and methanol under solvothermal conditions to give a solvated TEMPO-bearing PCP (DT-PCP; $[Zn_2(L1)_2(L2)](solvent)_n$) as orange platelet crystals (Figure S5). In view of the design of the dual TEMPO-bearing ligands, we expected DT-PCP to exhibit a high density of TEMPO radicals and thus show high catalytic activity. Single-crystal X-ray diffraction (SXRD) analysis revealed that DT-PCP exhibited a pillared-up three-dimensional (3D) framework structure (Figure S6). In as-synthesized DT-PCP (DT-PCP-DMF), the relatively large thermal ellipsoid of the TEMPO unit on the L1 ligand suggests the disordered nature of the TEMPO unit, featuring their unclear location. However, when the trapped DMF was exchanged for acetone, all mobile substituents became fixed in location (Figure 1b). Specifically, the paddlewheel zinc complex composed of $L1^{2-}$ and Zn^{2+} formed 2D sheets with a grid size of 19.4 Å × 19.4 Å (Figure 1c) that were further connected by the coordination of the pyridyl moieties in L2 to afford a 3D pillared layer structure with an interlayer distance of 17.74 Å (Figure 1d). The two interpenetrating 3D networks afforded channels along the *b* and *c* axises that accommodated the radical substituents of L1 and L2 (Figures 1e and 1f).

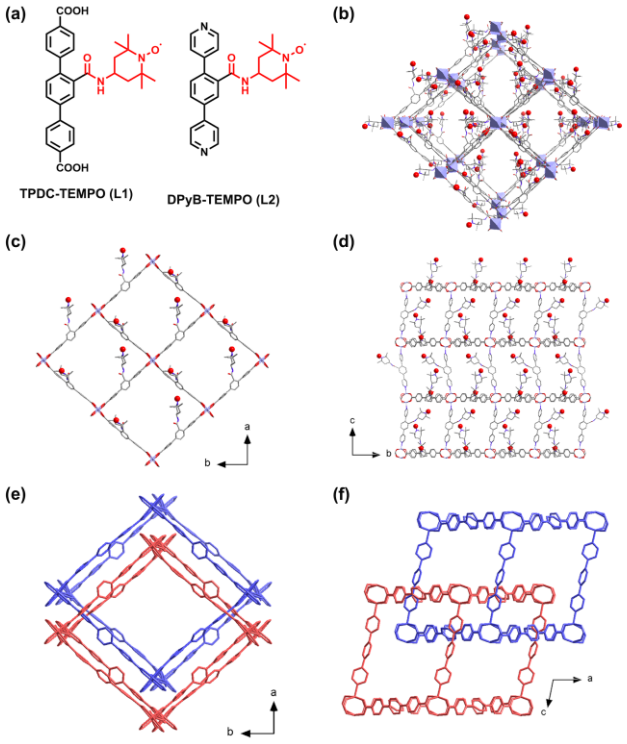

Figure 1. Structures of TEMPO-containing ligands and DT-PCP-acetone. (a) Ligands L1 and L2. (b) Single subnetwork of DT-PCP-acetone. Single layer (c) top and (d) side views of DT-PCP-acetone subnetwork. (e, f) Views of two-fold interpenetrating DT-PCP-acetone networks. Substituents are omitted for clarity.

Prior to thermal activation, the in-pore high-boiling-point DMF was exchanged for the volatile dichloromethane (DCM). Thermogravimetric analysis and nuclear magnetic resonance (NMR) spectroscopy confirmed the exhaustive solvent exchange and DCM removal below 100 °C (Figures S7 and S8). The PCP obtained after a solvent exchange with DCM and subsequent thermal activation at 80 °C (DT-PCP-TH) was examined by EPR spectroscopy to evaluate TEMPO activity (Figure S9). The EPR spectrum of DT-PCP-TH was similar to that of as-synthesized DT-PCP-DMF, displaying two symmetric sharp peaks centered between 3330 and 3340 G. The two peaks of DT-PCP-DMF and DT-PCP-TH covered the ligand triple peaks and were centered at the same *g*-value of 2.004, which showed that TEMPO activity was retained after incorporating into PCP framework (Figure S9). The structural flexibility of DT-PCP was verified by comparing the PXRD patterns of DT-PCP-TH and DT-PCP-DMF. After guest (DMF) removal, the diffraction peak at 2θ = 4.63° shifted to 4.98°, revealing the occurrence of guest-dependent structural changes (Figures S10a and b). The above results indicated that despite skeleton deformation after guest removal, the PCP maintained its crystalline nature and radical activity. Thus, DT-PCP was concluded to be the first example of a stable and flexible TEMPO radical–bearing PCP. The chemical stability of DT-PCP was evaluated by PXRD analysis after immersion in various organic solvents and strong base/acid for 24 h (Figure S10 c and d). DT-PCP maintained its crystallinity in common organic solvents and even in 1M HCl. While, in 1M NaOH and 1M HNO_3, DT-PCP was degraded severely.

The porosity of DT-PCP-TH was examined by gas sorption isotherm measurements of N_2 (77 K), O_2 (92 K), and CO_2 (195 K). DT-PCP-TH exhibited negligible N_2 and O_2 sorption but a significant CO_2 uptake of 87.5 $cm^3\ g^{-1}$ (Figure S11). Subsequently, we explored the ability of DT-PCP-TH to adsorb vapors of various polar solvents (Figure S12). In the case of DCM vapor uptake, we observed a step-shaped adsorption curve typical of flexible PCPs, revealing that the adsorption capacity reached 72.7 $cm^3\ g^{-1}$ at 21 kPa and sharply increased to 207.7 $cm^3\ g^{-1}$ at 55 kPa upon pore expansion. The adsorption of H_2O and MeOH did not display the step-shaped isotherms, but their adsorption capacities in the low-pressure range are larger than that of DCM uptake (Figure S12). This observation indicates that the interaction between H_2O/ MeOH molecules and framework is large enough to exhibit the framework deformation at a small pressure region to accommodate guest molecules.

To further prove the structural flexibility of DT-PCP, we conducted SXRD analyses on the solvated DT-PCP using different solvents, such as acetonitrile (ACN), acetone, DCM, or toluene (Table S1). The resulting framework exhibits an isomorphous structure, although the degree of dislocation and deformation of the framework depends on the solvents (Figure 2). The degree of the dislocation (Δ in Figure 2a) between the interpenetrating framework changed from 4.2 Å in ACN to 5.3 Å in DCM (Figures 2a and 2c). As a result, the diameter of the 1D channel along the *c*-axis (channel 1) decreased from 14.67 Å in ACN to 13.78 Å in DCM (blue points in Figure 2c). At the same time, the β angle changed from 101.4 ° in ACN to 104.2 ° in DCM, resulting in the decrease in the channel size along *b*-axis (channel2) from 8.65 in ACN to 8.32 Å in DCM. Thus, the channel

sizes of the solvated framework increased with decreasing solvent polarity. Structural analyses on the solvated samples confirmed that the configuration of DT-PCP was solvent-dependent and suggested that the relationship between configuration and solvent polarity can be used to control pore size.

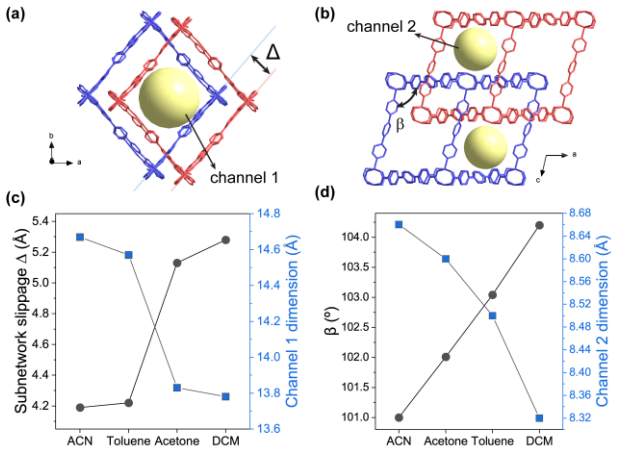

Figure 2. Structural changes of DT-PCP in different solvents, as determined from single-crystal X-ray diffraction data. The interpenetrating framework defines channels along with the (a) *c* and (b) **b** axes. Δ is the relative distance between the two interpenetrating subnetworks and β is the angle between L2 pillar ligands and the $(Zn_2L1_2)_n$ layers. (c, d) Effects of solvent on the unit cell parameter and channel dimension of DT-PCP obtained from single-crystal structures (120 K).

Owing to the TEMPO-bearing framework, we expect DT-PCP to exhibit catalytic nature for aerobic alcohol oxidation. Further, due to its solvent-dependent flexibility, we postulate that the solvent-dependent channel sizes of DT-PCP would make it promising for controllable size-selective catalysts. To compare the catalytic performance in different solvents, we set the reaction temperature to 35 °C, which is below the boiling point of DCM (40 °C), although TEMPO-catalyzed reactions are typically investigated at 80 °C.[25–28]

Initially, we examined the aerobic oxidation of benzyl alcohol (BnOH) in ACN, in which DT-PCP exhibits a large-pore conformation, and observed quantitative conversion to benzaldehyde (BnCHO) after 24 h (Table S2). The substrate scope was further investigated for a range of aromatic alcohols (Table S2) and all the tested alcohols were found to be quantitatively oxidized to the corresponding aldehydes. These results indicate that DT-PCP can efficiently catalyze aerobic alcohol oxidation at 35 °C, whereas previously reported TEMPO-bearing PCPs[25–28] require a temperature of 80 °C. The heterogeneous nature of our catalyst was confirmed using a hot filtration test. Specifically, DT-PCP was filtered out after the catalytic reaction, the filtrate was supplemented with BnOH, and the reaction was continued. NMR analysis showed a negligible conversion of BnOH after 24 h, indicating no leaching of the TEMPO moiety (Figure S13). Additionally, the catalyst recyclability test showed that DT-PCP retained its activity after reuse, although a certain crystallinity and activity degradation was observed in the third cycle (Figures S15 and S16).

After the catalytic activity was confirmed at 35 °C in ACN, we examined size-selective catalytic performance using solvents of various polarities as pore size switches and aromatic alcohols of different sizes (BnOH and 1-naphthol (NaphOH)) as size probes. The SXRD data of DT-PCP-toluene (Figure 3) suggest that the accommodation of guests with benzene segments requires the diameter of channel 2 to exceed 8.50 Å. DT-PCP-ACN and -acetone offer channels sufficiently large for this purpose, while DT-PCP-DCM exhibits channels that are narrower than required (Figures 3b, c). Thus, we assumed that BnOH could not enter the channels of DT-PCP-DCM but could enter the channels of DT-PCP-acetone/ACN.

Figure 3 presents the results of catalytic performance evaluation for DT-PCP in ACN, acetone, and DCM. After 24 h at 35 °C, DT-PCP-ACN quantitatively (yield > 99%) converted BnOH to BnCHO, while a BnCHO yield of 83.7% was obtained for DT-PCP-acetone after 36 h, and a low BnCHO yield of 14.5% was observed for DT-PCP-DCM at an extended reaction time of 48 h. According to the channel size comparison in Figure 2, we attributed the sluggish catalytic efficiency in acetone to limited pore accessibility. Compared with that of DT-PCP-toluene, channel 2 of DT-PCP-acetone is sufficiently large for BnOH entrance, while channel 1 is too small for aromatic substrate diffusion. Thus, only 2/3 of the channels in DT-PCP-acetone are available for BnOH adsorption and the in-pore catalytic reaction, which leads to lower BnOH conversion. The substrate BnOH cannot enter the DT-PCP-DCM pores to access the in-pore catalytic sites. Thus, the 14.5% BnOH conversion in DCM would be attributable to the surface catalytic sites.[30]

To further clarify the configuration dependency, we examined the NaphOH oxidation reaction under similar conditions. In ACN, NaphOH was quantitatively transformed to the corresponding aldehyde (NaphCHO) in 24 h, whereas yields of 42.5 and 0.5% were obtained after 48 h in acetone and DCM, respectively (Figure 3). The comparison between the aromatic substrate and the PCP channel dimensions indicates that the solvent-dependent channel size is correlated with their catalytic performance. Specifically, DT-PCP-ACN is a non-selective catalyst that can accommodate both BnOH and NaphOH for catalytic reactions. DT-PCP-acetone works as a size-selective catalyst because its channels can accommodate the relatively small substrate (BnOH), but exclude the large substrate (NaphOH). For DT-PCP-DCM, the compacted pores result in poor accessibility of any substrate, leading to poor catalytic activity.

TEMPO-bearing UIO-67 was reported as the only size-selective TEMPO-PCP catalyst, achieving size selection via the rigid pore sieving effect.[30] DT-PCP is characterized by its controllable selectivity. Flexibility allows this material to act either as a non-selective catalyst converting all substrates in the mixture or as a size-selective catalyst with a preference for small substrates. Lastly, it is worth noting that TEMPO density in the reporting PCP can be manipulated via the ligand substitution. We designed an inert ligand, N-cyclohexyl-2,5-di(pyridin-4-yl)benzamide (CDPB), which substituent is of a similar structure to the TEMPO (inset of Figure S24). A new PCP (TCycH-PCP), composed of CDPB and TPDC-TEMPO ligand, is isostructural to DT-PCP (Figure S24). This result implies the potential use of our system to investigate various catalytic reactions with optimizing the radical concentration in the framework.

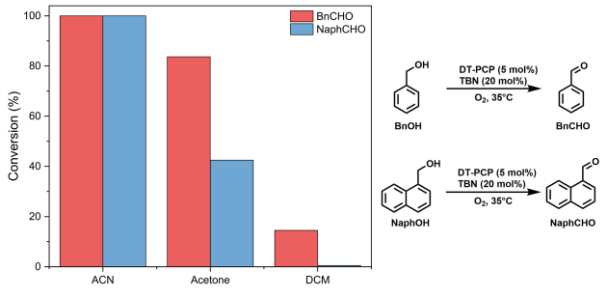

Figure 3. Conversion rates of alcohols in different solvents after the aerobic oxidation using DT-PCP at 35 °C. The conversion of BnOH was obtained after reacting in ACN for 24 h, 36 h in acetone, and 48 h in DCM. For NaphOH, the conversion was calculated after reacting in ACN for 24 h, 48 h in acetone, and DCM.

In summary, we synthesized a flexible PCP with a high density of TEMPO substituents (DT-PCP) and examined its structural flexibility by SXRD, revealing that the pore conformation can be controlled through the choice of solvent. This structural flexibility was used to control the accessibility of TEMPO sites to aromatic alcohols during their aerobic oxidation. The large-pore conformation of DT-PCP in the highly polar ACN allowed the catalytic conversion of aromatic substrates with varied sizes and properties, whereas the contracted-pore conformation observed in the low-polarity acetone allowed small substrates to be converted in preference to larger ones. Thus, the solvent-responsive flexibility of DT-PCP makes it a promising size-selective catalyst.

This work was supported by the KAKENHI Grant-in-Aid for Scientific Research (S) (JP18H05262, JP22H05005) and (C) (JP22K05128) from the Japan Society of the Promotion of Science (JSPS). KO acknowledges the support from ISHIZUE 2021 of the Kyoto University Research Development Program and "Innovation Inspired by Nature" Research Support Program, SEKISUI CHEMICAL CO., LTD. Synchrotron X-ray measurements were supported by the Japan Synchrotron Radiation Research Institute (JASRI) (Proposal No. 2021A1104, 2021B1528, 2022A1500). We thank the iCeMS analysis center for the access to the analytical instruments. Profs. H.Kitagawa and K. Otsubo (Kyoto University) are acknowledged for providing access to EPR instrument.

Conflicts of interest

There are no conflicts to declare.

References

1 S. Kitagawa and M. Kondo, *Bull. Chem. Soc. Jpn.*, 1998, **71** , 1739.
2 S. Horike , S. Shimomura and S. Kitagawa, *Nat. Chem.*, 2009, **1** , 695.
3 X. Chen, H. Xie, E. R. Lorenzo, C. J. Zeman, Y. Qi, Z. H. Syed, A. E. B. S. Stone, Y. Wang, S. Goswami, P. Li, T. Islamoglu, E. A. Weiss, J. T. Hupp, G. C. Schatz, M. R. Wasielewski, and O. K. Farha, *J. Am. Chem. Soc.*, 2022, **144**, 6, 2685–2693.
4 Z.-Q. Yao, K. Wang, R. Liu, Y.-J. Yuan, J.-J. Pang, Q. W. Li, T. Y. Shao, Z. G. Li, R. Feng, B. Zou, W. Li, J. Xu, and X.-H. Bu, *Angew. Chem. Int. Ed.,* 2022, **61**, e202202073.
5 W. Meng, S. Kondo, T. Ito, K. Komatsu, J. Pirillo, Y. Hijikata, Y. Ikuhara, T. Aida, and H. Sato, *Nature,* 2021, **598**, 298–303.
6 X.-W. Zhang, D.-D. Zhou, and J.-P. Zhang, *Chem,* 2021, **7**, 1006–1019.
7 P. Wang, K.-i. Otake, N. Hosono, and S. Kitagawa, *Angew. Chem. Int. Ed.,* 2021, **60**, 7030–7035.
8 B.-Q. Song, Q.-Y. Yang, S.-Q. Wang, M. Vandichel, A. Kumar, C. Crowley, N. Kumar, C.-H. Deng, V. GasconPerez, M. Lusi, H. Wu, W. Zhou, and M. J Zaworotko, *J. Am. Chem. Soc.,* 2020, **142**, 6896–6901.
9 Y. Gu, J.-J. Zheng, K.-i. Otake, K. Sugimoto, N. Hosono, S. Sakaki, F. Li, and S Kitagawa,. *Angew. Chem. Int. Ed.,* 2020, **59**, 15517 –15521**.**
10 T. Kundu, M. Wahiduzzaman, B. B. Shah, G. Maurin, and D. Zhao, *Angew. Chem. Int. Ed.,* 2019, **58**, 8073–8077.
11 S. Kusaka, A. Kiyose, H. Sato, Y. Hijikata, A. Hori, Y. Ma, and R. Matsuda, *J. Am. Chem. Soc.,* 2019, **141**, 15742–15746.
12 M. Souto, J. Romero, J. Calbo, I. J. Vitórica-Yrezábal, J. L. Zafra, J. Casado, E. Ortí, A. Walsh, and G. Mínguez Espallargas, *J. Am. Chem. Soc.,* 2018, **140**, 10562–10569.
13 C. Gu, N. Hosono, J.-J. Zheng, Y. Sato, S. Kusaka, S. Sakaki, and S. Kitagawa, *Science,* 2019, **363**, 387–391.
14 S. Krause, N. Hosono, and S. Kitagawa, *Angew. Chem. Int. Ed.,* 2020, **59**, 15325–15341.
15 F. Bigdeli, C. T. Lollar, A. Morsali, and H. C. Zhou, *Angew. Chem. Int. Ed.,* 2020, **59**, 4652–4669.
16 S. K. Elsaidi, M. H. Mohamed, D. Banerjee, and P. K. Thallapally, *Coord. Chem. Rev.,* 2018, **358**, 125–152.
17 T. D. Bennett, A. K. Cheetham, A. H. Fuchs, and F.-X. Coudert, *Nat. Chem.,* 2017, **9**, 11–16.
18 C. Ze, Y. Dong-Hui, X. Jian, H. Tong-Liang, and B. Xian-He, *Adv. Mater.,* 2015, **27**, 5432–5441.
19 A. Schneemann, V. Bon, I. Schwedler, I. Senkovska, S. Kaskel, and R. A. Fischer, *Chem. Soc. Rev.,* 2014, **43**, 6062–6096.
20 J. Y. Lee, O. K. Farha, J. Roberts, K. A. Scheidt, S. T. Nguyena, and J. T. Hupp, *Chem. Soc. Rev.*, 2009, **38**, 1450–1459.
21 K. Otake, Y. Cui, C. T. Buru, Z. Li, J. T. Hupp, and O. K. Farha, *J. Am. Chem. Soc.,* 2018, **140**, 8652-8656.
22 Y. -B. Huang, J. Liang, X. -S. Wanga, and R. Cao, *Chem. Soc. Rev.*, 2017,**46**, 126–157.
23 Y. Zhang, X. Zhang, J. Lyu, K. -i. Otake, X. Wang, L. R. Redfern, C. D. Malliakas, Z. Li, T. Islamoglu, B. Wang, and O. K. Farha, *J. Am. Chem. Soc.,* 2018, **140**, 36, 11179–11183.
24 Z. Ma, K. T. Mahmudov, V. A. Aliyeva, A. V. Gurbanov, A. J. L. Pombeiro, *Coord. Chem. Rev.*, 2020, **423**, 213482.
25 L. Li , R. Matsuda, I. Tanaka, H. Sato, P. Kanoo, H. J. Jeon, M. L. Foo, A. Wakamiya, Y. Murata, and S. Kitagawa, *J. Am. Chem. Soc.*, 2014, **136**, 7543–7546.
26 K. M. Zwoliński, and M. J. Chmielewski , *ACS Appl. Mater. Interfaces*, 2017, **9** , 33956–33967.
27 J. L. Zhuang, X. Y. Liu, Y. Zhang, C. Wang, H. L. Mao, J. Guo, X. Du, S.-B. Zhu, B. Ren, and A. Terfort, *ACS Appl. Mater. Interfaces*, 2019, **11**, 3034–3043.
28 Z. Li, Y. Liu, X. Kang, and Y. Cui, *Inorg. Chem.*, 2018, **57**, 9786–9789.
29 M. J. Jellen, M. J. Ayodele, A. Cantu, M. D. E. Forbes, and M. A. Garcia-Garibay, *J. Am. Chem. Soc.*, 2020, **142**, 18513–18521.
30 S. Kim, J. Lee, S. Jeoung, H. R. Moon, and M. Kim, *Chem. Eur. J.* 2020, **26**, 7568-7572.